Modeling the Influence of Decomposing Organic Solids on Sulfate Reduction Rates for Iron Precipitation

P A U L O   S .   H E M S I , [†]
C H A R L E S   D .   S H A C K E L F O R D , * , [†]   A N D
L I N D A   A .   F I G U E R O A [‡]

*Department of Civil Engineering, Colorado State University,
Fort Collins, Colorado 80523-1372, and Division of
Environmental Science and Engineering, Coolbaugh Hall,
Colorado School of Mines, Golden, Colorado 80401-1887*

The influence of decomposing organic solids on sulfate
(SO_4^{2-}) reduction rates for metals precipitation in sulfate-
reducing systems, such as in bioreactors and permeable
reactive barriers for treatment of acid mine drainage,
is modeled. The results are evaluated by comparing the
model simulations with published experimental data for two
single-substrate and two multiple-substrate batch
equilibrium experiments. The comparisons are based on
the temporal trends in SO_4^{2-}, ferrous iron (Fe^{2+}), and hydrogen
sulfide (H_2S) concentrations, as well as on rates of
sulfate reduction. The temporal behaviors of organic solid
materials, dissolved organic substrates, and different
bacterial populations also are simulated. The simulated
results using Contois kinetics for polysaccharide decomposi-
tion, Monod kinetics for lactate-based sulfate reduction,
instantaneous or kinetically controlled precipitation of ferrous
iron mono-sulfide (FeS), and partial volatilization of H_2S
to the gas phase compare favorably with the experimental
data. When Contois kinetics of polysaccharide decomposition
is replaced by first-order kinetics to simulate one of
the single-substrate batch experiments, a comparatively
poorer approximation of the rates of sulfate reduction is
obtained. The effect of sewage sludge in boosting the short-
term rate of sulfate reduction in one of the multiple-
substrate experiments also is approximated reasonably
well. The results illustrate the importance of the type of
kinetics used to describe the decomposition of organic solids
on metals precipitation in sulfate-reducing systems as
well as the potential application of the model as a predictive
tool for assisting in the design of similar biochemical
systems.

Introduction

A number of laboratory experiments have demonstrated
remediation of acid mine drainage (AMD) based on sulfate
(SO_4^{2-}) reduction and metal−sulfide precipitation. Examples
of the solid, decomposable organic materials that have been
evaluated for this purpose include sawdust (*1, 2*), spent
mushroom compost (*3, 4*), fresh alfalfa (*5*), whey/cow manure
(*6*), leaf compost/sewage sludge (*7*), spent mushroom
compost/oak chips/wastepaper sludge (*8*), leaf compost/
sawdust/wood chips/sewage sludge (*9, 10*), leaf compost/
wood chips/poultry manure (*11*), wood chips/pulp and paper
waste (*12*), and wheat straw (*13*), among others. In some
cases, organic solid materials have been amended with
dissolved organic substrates (*5, 13*).

Several studies involving field applications of sulfate-
reducing (SR) systems for remediation of AMD in the form
of permeable reactive barriers (PRBs) and bioreactors also
have been reported (*14−19*). For example, an SR−PRB
containing 50% gravel, 20% municipal compost, 20% leaf
mulch, 9% wood chips, and 1% limestone, all by volume,
was constructed in 1995 at the Nickel Rim mine in Ontario,
Canada (*15−17*), and after three years of operation, SO_4^{2-}
removal declined by ~30% and Fe^{2+} removal declined by
~50%.

With respect to mathematical modeling of the rate of
sulfate reduction in SR systems, Bourdeau and Westrich (*20*)
and Westrich and Berner (*21*) considered aerobic degradation
of seawater plankton as a precursor to sulfate reduction in
marine environments, suggesting first-order kinetics with
respect to carbon as a model for the rates of plankton
degradation and SO_4^{2-} reduction, the latter also including a
hyperbolic term to account for SO_4^{2-} limitation. Drury (*22*)
developed a model that assumes the rate of sulfate reduction
in anaerobic solid-substrate bioreactors to be proportional
to the rate of decomposition of biodegradable solid waste
materials (e.g., manure, compost, wood chips) initially added
to the bioreactor (without replenishment of organic carbon).
Drury (*22*) modeled the degradation of solid organic materials
using first-order kinetics with a declining rate coefficient
(*23, 24*) based on an empirical model that equates the rate
of sulfate reduction to conversion factors multiplied by the
rate of solid decomposition and by the concentration of SO_4^{2-}.
However, neither Bourdeau and Westrich (*20*) nor Drury (*22*)
considered the possibility of Monod kinetics (*25*) for
sulfate reduction, the dynamics of bacterial populations
(i.e., decomposers and SR bacteria, SRB), or the effects of
bacterial growth and decay. Dissolved organic electron
donors existing as the products of hydrolysis/fermentation
reactions and utilizable as SRB substrates (*26, 27*) also were
not considered.

Mayer et al. (*28*) describe the conceptual framework of a
reactive transport model that includes kinetically controlled
pyrrhotite oxidation by O_2 and Fe^{3+}, transport of AMD species
impacted by equilibrium with a number of aluminosilicate
and carbonate minerals, as well as the sulfate mineral
gypsum, and remediation based in part on kinetically
controlled sulfate reduction, although the kinetic equations
for sulfate reduction and substrate consumption were not
provided. However, the model proposed by Mayer et al. (*28*)
does not handle bacterial populations (e.g., decomposers
and SRB) or the effects of bacterial growth and decay. The
model also does not consider kinetic expressions for de-
composition of solid organic materials or the kinetics of
dissolved organic substrates required for sulfate reduction.

Prommer et al. (*29*) describe a reactive transport model
based on MODFLOW (*30*), MT3DMS (*31*), and the equilibrium
geochemical model PHREEQC-2 (32) that can handle both
equilibrium and kinetically controlled reactions. An applica-
tion of the model involving treatment of AMD containing
SO_4^{2-} and Zn^{2+} is described, whereby the rate of sulfate
reduction is modeled considering Monod kinetics and
including bacterial growth and decay, although the actual
kinetic expressions are not given. However, the model does

* Corresponding author phone: (970)491-5051; fax:
(970)491-3584; e-mail: shackel@engr.colostate.edu.
† Colorado State University.
‡ Colorado School of Mines.

not consider solid decomposable organic materials, and the application is based on an injected treatment zone created by injection wells in which a dissolved organic substance (ethanol) is introduced in the subsurface to promote the growth of SRB, H_2S production, and precipitation of ZnS.

Benner et al. (33) and Amos et al. (34) describe a simplified model for the rate of sulfate reduction for AMD remediation in which a constant rate of sulfate reduction is multiplied by a hyperbolic term that accounts for SO_4^{2-} limitation (20). This model does not consider the bacterial population (i.e., neglects the effects of bacterial growth and decay), and the sulfate reduction rate in the model is assumed to be constant with a reduction rate that is based on a priori fitting to measured sulfate data, e.g., from the effluent of a column test (34). This proposed approach is empirical and potentially oversimplifies sulfate reduction, since the rate of sulfate reduction typically is limited by the concentration of dissolved organic electron donors/SRB substrates associated with solid decomposition and also is linked to the growth of the SRB population (3, 5, 8, 20−22).

The objective of this study is to model the influence of decomposing organic solids on sulfate reduction rates for the purpose of describing the precipitation of iron in SR systems. The simulated results are obtained using a new mathematical model in which sulfate reduction kinetics are coupled to, and limited by, the decomposition of solid organic materials and simultaneously combining meaningful biochemical processes not combined in any of the aforementioned models. Experimental results taken from the literature are used as the basis for calibrating parameter values (initially taken from the literature) used in the simulations and subsequently validating the ability of the model to describe the influence of decomposing organic solids on sulfate reduction rates for ferrous iron (Fe^{2+}) precipitation.

System Analyses

Simulated results for SO_4^{2-}, Fe^{2+}, and H_2S in solution are compared with experimental results for the same species based on four batch-test experiments reported by Waybrant et al. (9) performed at room temperature, which is assumed as 25 °C. The experimental results are derived from two single-substrate (i.e., one containing delignified waste cellulose and one containing composted leaf mulch compost) and two multiple-substrate (i.e., one containing leaf mulch/sawdust and one containing leaf mulch/sawdust/wood chips/sewage sludge) batch tests. Simulations of solid decomposable organic materials, dissolved organic substrates, and different populations of bacteria also are included but are not compared with experimental results since no such results were reported. The solid phases consisting of the decomposable polysaccharide and the bacterial populations are assumed uniformly dispersed in the liquid phase (i.e., batch experiments are continuously mixed).

Although Zn^{2+} was present in some of the batch tests at initial concentrations of ∼0.8 mg/L (i.e., ∼0.1%, mg/L basis, of those for Fe^{2+}), Zn^{2+} precipitation with H_2S was assumed to be negligible relative to that for Fe^{2+}. Also, although Ni^{2+} was present in some batch tests at initial concentrations of ∼1.1 mg/L (i.e., ∼0.1%, mg/L basis, of those for Fe^{2+}) and Cd^{2+} and Pb^{2+} were spiked in some batch tests, the simulations of these metals are not considered because (i) no quantitative monitored data are provided for these elements, (ii) the reported initial concentrations are low relative to those for Fe^{2+}, and (iii) the life spans of these metals in the systems are only ∼10% of the total testing time. Finally, although Na^+, K^+, and Mg^{2+} were monitored in the experiments, the temporal behaviors of these metals were not simulated because these metals are not included within the scope of the model used to perform the simulations.

Significant, abrupt declines in the concentrations for SO_4^{2-} and Fe^{2+} are reported in ref 9, particularly in the case of Fe^{2+}, apparently at time equal to zero (i.e., immediately after the mixing of solids/batch solution). These abrupt declines in the concentrations for SO_4^{2-} and Fe^{2+} may be attributed to either (i) instantaneous sulfate reduction based on a dissolved available substrate, and/or (ii) sorption to the solid organic materials. If lactate is taken as representative of the dissolved substrates, then different stoichiometric amounts of lactate would be required at time zero in order to justify the declines in both Fe^{2+} and SO_4^{2-} per batch test, suggesting that the presence of lactate at time zero cannot be used to explain both declines. For example, for the leaf mulch/sawdust batch test, the decline in Fe^{2+} is 507 mg/L, which would require 1720 mg/L lactate, whereas the decline in SO_4^{2-} is 400 mg/L, which would require 790 mg/L lactate. As a result, the simulations in this study focus on the longer-term behavior of SR systems based on the decomposition of solid substrates, and sulfate reduction based on dissolved substrates possibly present at time zero is neglected.

With respect to sorption, Fe^{2+} is more likely than SO_4^{2-} to undergo instantaneous (and reversible) sorption to the negatively charged surfaces of organic materials (35). However, sorption was not evaluated by Waybrant et al. (9) and similarly is not considered in this study. Thus, declines in Fe^{2+} concentrations that are presumably not related to SO_4^{2-} reduction and metal−sulfide precipitation are not considered in this study.

The initial pH of each batch mixture was reported in ref 9 to range from 5.5 to 6.5, and the pH was maintained consistently within the range from 6.5 to 7.5 after the start of sulfate reduction, which is compatible with the pH range of 6−7 assumed for speciation in this study. The SO_4^{2-} concentrations in the system are affected by gypsum ($CaSO_4 \cdot 2H_2O$) dissolution, since gypsum was added to the creek sediment in the tests. However, this process was not considered in the evaluation of sulfate reduction rates in ref 9 because the contribution of gypsum to the measured SO_4^{2-} concentrations could not be isolated. Therefore, this process also is not considered in the simulations performed in this study.

With respect to precipitation of Fe^{2+}, sulfate reduction and precipitation of FeS and $FeS_{0.9}$ (mackinawite) was reported in ref 9 to have controlled Fe^{2+} removal from the time when sulfate reduction became active (∼20 days) until Fe^{2+} depletion (∼80 days). Geochemical modeling based on measured concentrations of Ca^{2+}, Fe^{2+}, HCO_3^-, and SO_4^{2-} reported in ref 9 indicated a tendency for the solution to be undersaturated with respect to calcite and oversaturated with respect to gypsum and siderite ($FeCO_3$) at earlier times (<20 days). After ∼20 days, this tendency reverts, and gypsum and siderite tend to dissolve and calcite tends to precipitate. Before sulfate reduction was active (<∼20 days), an unknown amount of Fe^{2+} may have precipitated as $FeCO_3$, but the geochemical modeling also suggests that Fe^{2+} would have returned to solution upon $FeCO_3$ dissolution after ∼20 days. The present simulations assume only FeS as the sink for Fe^{2+}, and the validity of this assumption will be addressed by comparing simulated and experimental Fe^{2+} trends.

Model Description

The simulations are based on a conceptual model that includes (i) anaerobic decomposition of polysaccharides in solid organic materials due to the activity of decomposer bacteria and producing lactate, (ii) sulfate reduction based on the incomplete oxidation of lactate, (iii) instantaneous or kinetically controlled precipitation of heavy-metal monosulfides, and (iv) partial volatilization of H_2S to the gas phase. The explanation of the conceptual basis for the model, description of biochemical processes, kinetic and mass

TABLE 1. Solids and Decomposable Organic Fraction Composition for Four Batch Experiments Reported in Ref 9

batch test	batch volume (mL)	solids (dry mass basis)				decomposable organic fraction (dry mass basis)					
		total		organic fraction			composition (g/L)				
		(g)	(g/L)	(%)	(g/L)	total	cellulose	leaf mulch	sawdust	wood chips	sewage sludge
1	959	117	122	19	23.2	18.6	18.6 (100%)				
2	466	77	165	27	44.5	22.3		22.3 (100%)			
3	897	128	143	31	44.3	22.2		13.3 (60%)	8.9 (40%)		
4	857	114	133	48	63.8	28.2		19.1 (60%)	3.2 (10%)	4.8 (15%)	1.1 (15%)

TABLE 2. Assumed Initial Concentrations of Sulfate, Ferrous Iron, Hydrogen Sulfide, Lactate, and Acetate for Four Batch Experiments Performed by Waybrant et al. (ref 9)

batch test	materials	initial concn (mg/L)				
		SO_4^{2-}	Fe^{2+}	H_2S	lactate	acetate
1	cellulose	4000	1110	0	0	0
2	leaf mulch	3480	510	0	0	0
3	leaf mulch/sawdust	4400	744	0	0	0
4	leaf mulch/sawdust/woodchips/sewage sludge	3300	200	0	0	0

balance equations, as well as explanations on the mathematical solution and verifications of mass balances and levels of numerical accuracy are provided in the Supporting Information.

Initial Conditions and Parameter Values. The volume of batch solution, total dry mass of solids (inorganic and organic), equivalent concentration of solids (i.e., dry mass of solid material per liter of batch solution), percentage and composition of organic solids with respect to the total mass of solids (by dry mass), and estimated initial amounts of decomposable polysaccharides (by dry mass) are shown for each batch test in Table 1. The distinction between the amounts of total organic solids and anaerobically decomposable polysaccharides is important. The estimated initial amounts of decomposable polysaccharides in each batch test of 50% (by dry mass) with respect to the total dry mass of leaf mulch, sawdust, and wood chips were based on a combination of representative percentages reported in the literature. For delignified waste cellulose, the decomposable cellulose content is expected to be closer to unity (e.g., 85%). Waybrant et al. (9) indicate that municipal sewage sludge has a carbon content that is significantly lower than the carbon content in cellulose, leaf mulch, sawdust, and wood chips (i.e., 0.093 g/g, by dry mass, vs values ranging from 0.35 to 0.47 g/g). Thus, the content of decomposable organic solids of generic formula CH_2O in municipal sewage sludge can be assumed to be proportionally lower. The content of decomposable solids in municipal sewage sludge was estimated as 12% on a dry mass basis.

The initial concentrations assumed for SO_4^{2-}, Fe^{2+}, H_2S, lactate ($C_3H_5O_3^-$), and acetate ($C_2H_3O_2^-$) for each batch test are shown in Table 2. Approximately 40–60% (by dry mass), or <15 vol %, of anaerobic creek sediment was mixed with the solid materials in each batch experiment to serve as bacterial source or inoculating material (9).

SRB that are incomplete oxidizers of lactate, such as *Desulfovibrio vulgaris*, are significantly more abundant than SRB that oxidize acetate or that are complete oxidizers of lactate (8, 36). The equivalent biomass concentration (by dry mass) of SRB that are incomplete oxidizers of lactate when sulfate reduction is active is estimated to range from 1 to 1000 mg biomass/L. This range is based on the abundance range of 10^7–10^9 cells/mL (12, 33), considering 10^{-10}–10^{-9} mg/cell by dry mass, i.e., cylindrical cells with ~2.35 μm of height and ~0.75 μm of diameter (37). The intermediate value of 50 mg biomass/L generally was used in simulations, corresponding to an abundance range from 5×10^7 to 5×10^8 cells/mL.

The estimated range for the equivalent biomass concentration (by dry mass) of cellulolytic/hemicellulolytic decomposing bacteria colonizing the decomposable polysaccharides ranges from 0.1 to 10 mg biomass/g of dry polysaccharide, based on the cell coverage range of ~10^9–10^{10} cells/g of dry detritus and considering 10^{-10}–10^{-9} mg/cell by dry mass (e.g., Fenchel and Harrison (38) report 5×10^{-10} mg/cell). The cell coverage is obtained from 2 to 15 cells/100 μm² of fiber of decomposable detritus (38, 39), assuming fibers of ~2 mm of diameter, 5 mm of length, and ~0.003 g/fiber. Values for the decomposer biomass concentration divided by the concentration of decomposable polysaccharide by dry mass, or $[X_d]/[CE]$, ranging from 2.75×10^{-3} to 1×10^{-2} were used for the simulations.

The parameter values used in different simulation cases for each batch test are shown in Table 3. In batch test 1, the first case (case 1a, Table 3) corresponds to parameter values from Vavilin et al. (40) for cellulose decomposition at 35 °C. Subsequent cases 1b and 1c reflect the adjustment of these parameters to 25 °C. In the case of leaf mulch, sawdust, and wood chips, decomposition parameter values were adjusted and compared, and once the parameter values for a given material were adjusted in a batch test, the same parameter values were kept for that material in the other batch test simulations. For sewage sludge, decomposition parameter values from Vavilin et al. (40) for 25 °C were used.

Parameter values for sulfate reduction via Monod kinetics based on lactate were obtained from the literature (41–43) and were maintained constant in the simulations in the present methodology, since the major emphasis in this study is placed on the effects of organic matter decomposition in SR systems (see Supporting Information). These parameter values included a maximum specific SRB growth rate, μ_{SRB}, of 4.0 d^{-1}, and half-saturation coefficients for lactate (K_V) and sulfate (K_{SO}) of 5.0 and 1.5 mg/L, respectively.

Results and Discussion

Batch Test 1. The simulated results of batch test 1 (batch mixture 8 in ref 9) containing decomposable, delignified waste cellulose at an estimated initial concentration of 18.6 g/L are compared to the experimental results in Figures 1–5. Simulated concentrations for SO_4^{2-}, Fe^{2+}, and H_2S vs batch reaction time are obtained considering Contois or first-order kinetic models for the decomposition of cellulose, Monod kinetics for lactate-based sulfate reduction, and instantaneous precipitation of FeS. In some cases, partial volatilization of H_2S to a periodically vented gas phase is considered.

TABLE 3. Parameter Values Used for Simulation Cases of the Results of the Four Batch Experiments Reported in Ref 9

| | | | decomposition | | | | precipitation | |
| | | | Contois kinetics | | | first-order | instantaneous | first-order |
batch test	case	materials	k_c (d^{-1})	K_c (g/g)	$[X_d]_i/[CE]_i$	k_f (d^{-1})		k (d^{-1})
1	1a	cellulose	1.25	7.5	0.0005, 0.00275, 0.005		yes	
	1b		0.625	37.5	0.0005, 0.00275, 0.005		yes	
	1c		0.625	30	0.0005, 0.00275, 0.005		yes	
	1d					0.02	yes	
	1e					0.01	yes	
	1f					0.005	yes	
2	2a	leaf mulch	0.625	30	0.00275, 0.005, 0.01		yes	
	2b		0.8	30	0.00275, 0.005		yes	
3	3a	leaf mulch + sawdust	0.625	30	0.01		yes	
	3b		0.8	30	0.005		yes	
	3c		0.8	30	0.005			0.1
	3d		0.8	30	0.005			0.0005
4	4a	leaf mulch + sawdust	0.625	30	0.01		yes	
		wood chips	0.4	30	0.005			
		sewage sludge	8.0	30	0.01			
	4b	leaf mulch + sawdust	0.8	30	0.005		yes	
		wood chips	0.4	30	0.005			
		sewage sludge	8.0	30	0.01			
	4c	leaf mulch + sawdust	0.8	30	0.005		yes	
		wood chips	0.4	30	0.005			
		sewage sludge	0.0					
	4d	leaf mulch + sawdust	0.0				yes	
		wood chips	0.0					
		sewage sludge	8.0	30	0.01			

Sulfate, Ferrous Iron, and Hydrogen Sulfide. Simulated SO_4^{2-} concentrations with time are compared to experimental results in Figure 1. As shown in Figure 1a, when parameter values from Vavilin et al. (40) for cellulose decomposition at 35 °C (case 1a, Table 3) are used, sulfate reduction is significantly over predicted. As a result, cellulose decomposition kinetics was adjusted to 25 °C by decreasing the decomposition rate constant by 50% for the 10 °C drop and increasing the half-saturation coefficient, K_c (44, 45). The temperature-adjusted parameter values (cases 1b and 1c, Table 3) result in much more favorable approximations of the experimental data (parts b and c of Figure 1), with the results using $K_c = 37.5$ g/g and $[X_d]/[CE] = 0.00275$ (case 1b, Figure 1b) providing the best, observed fit to the experimental data. Accordingly, the simulated Fe^{2+} and H_2S concentrations were compared to the experimental Fe^{2+} and H_2S concentrations, respectively, using the parameter values for case 1b. As shown in Figure 2a, the simulated Fe^{2+} concentrations compare favorably with the experimental data for the case where $K_c = 37.5$ g/g and $[X_d]/[CE] = 0.00275$ (case 1b, Table 3), i.e., case 1b provides favorable SO_4^{2-} and Fe^{2+} approximations. Since the instantaneous-precipitation algorithm resulted in good approximations of Fe^{2+} concentrations vs time, the kinetically controlled (first-order kinetics) model for precipitation was not used for this case.

However, the cumulative concentrations of H_2S in solution with no volatilization shown in Figure 2b far exceed the experimental results after depletion of Fe^{2+} but are in agreement with the sulfur mass balance for the system. For example, up to 124 days (SO_4^{2-} depletion), ~1418 mg of H_2S has been released by sulfate reduction and ~671 mg H_2S has been precipitated as FeS, thus requiring ~747 mg H_2S to remain in solution if no volatilization of H_2S is considered (Figure 2b). The headspace gas phase of the reaction flask was vented periodically to allow excess gas to escape, which is presumably a requirement for closing the sulfur mass balance for the results reported in ref 9. As a result, three simulations were performed assuming different values for the unknown frequency of headspace venting (i.e., once every one, two, or three days) and a dimensionless Henry's law

coefficient for H_2S of 0.53 (45), as shown in Figure 2b. The simulations including volatilization show that the measured H_2S concentrations may be realistic assuming that volatilization was allowed periodically.

Rates of Sulfate Reduction and Precipitation. Simulated rates of sulfate reduction with time are compared in Figure 3 to rates calculated from the SO_4^{2-} data in ref 9 considering either Contois decomposition kinetics (cases 1a, 1b, and 1c, Table 3) as shown in Figure 3a or first-order decomposition kinetics (cases 1d, 1e, and 1f) as shown in Figure 3b. Simulated rates of sulfate reduction for Contois kinetics using a rate coefficient, k_c, of 1.25 d^{-1} and a half-saturation coefficient, K_c, of 7.5 g/g (case 1a) are significantly higher than the experimental data, whereas those using half the value for k_c (i.e., 0.625/d) and K_c of either 37.5 g/g (case 1b) or 30.0 g/g (case 1c) provide good approximations of the experimental data, except for the period between ~60 and 70 days, where an abrupt decline in the experimental rate of sulfate reduction occurs. Such abrupt discontinuities in the experimental data generally cannot be simulated using the current model, which is based on continuous functions that predict smooth trends in data (i.e., without changing initial conditions).

The simulated results based on first-order decomposition kinetics (cases 1d, 1e, and 1f, Figure 3b) predict the rate of sulfate reduction to be at the maximum value at time zero and decline monotonically with time. However, this behavior contradicts the experimental behavior in which the rate of sulfate reduction reaches a maximum value only several days after the beginning of the experiment. Therefore, Contois kinetics appears to be a preferable model for the decomposition of organic solids in this SR system, with the Contois parameter values corresponding to case 1b (i.e., $k_c = 0.625$/d, $K_c = 37.5$ g/g, and $[X_d]/[CE] = 0.00275$) resulting in the best comparisons with the experimental data.

Accordingly, the simulated rates of cellulose decomposition, sulfate reduction, and Fe^{2+} precipitation for the Contois parameter values associated with case 1b are shown in Figure 4. The results in Figure 4 show that sulfate reduction rates increase with increasing rates of cellulose decomposition
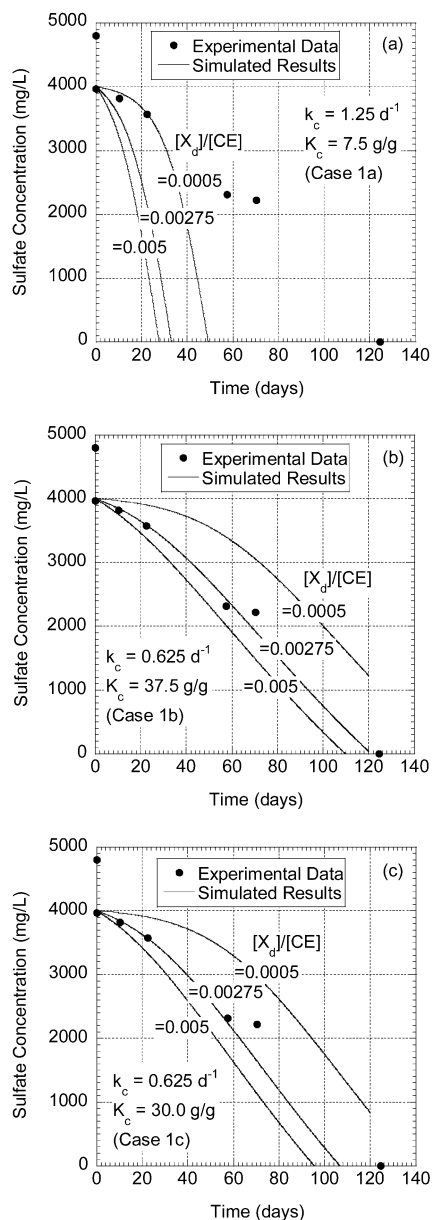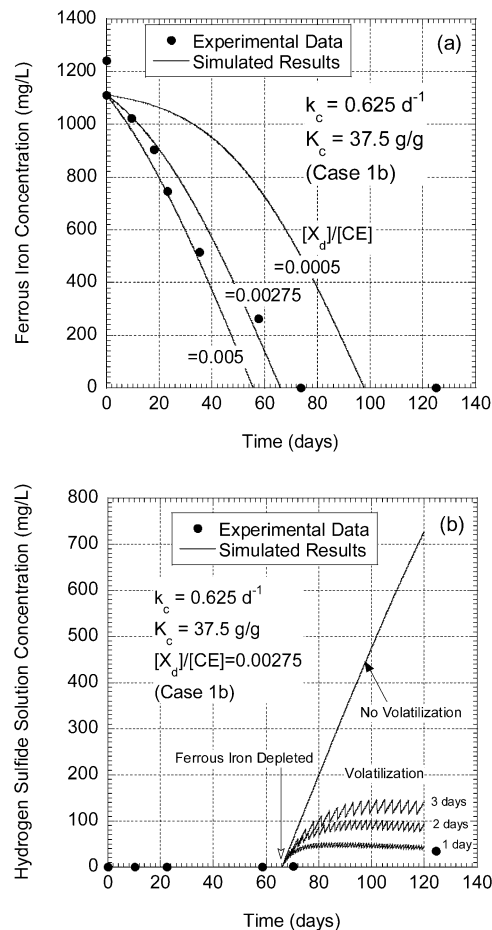
FIGURE 1. Comparison of experimental and simulated sulfate concentrations based on Contois decomposition kinetics for batch test 1 (k_c = decomposition rate coefficient; K_c = half-saturation coefficient; $[X_d]/[CE]$ = initial concentration ratio of decomposer bacteria to polysaccharide).

before SO_4^{2-} becomes limiting to sulfate reduction. Between 73 and 124 days, the rates of sulfate reduction decline, first as a result of the declining rate of cellulose decomposition and finally due to the depletion of SO_4^{2-}. The simulated rates of Fe^{2+} precipitation follow an analogous relationship (i.e., increase with increasing rates of cellulose decomposition) until 66 days when Fe^{2+} is depleted from the system and the rates of Fe^{2+} precipitation decline abruptly and independently from the rate of cellulose decomposition.

Cellulose, Decomposer Bacteria, and SRB. The simulated results for the percentage of the initial decomposable cellulose remaining and concentrations of decomposer bacteria for the Contois kinetics case 1b are shown in Figure 5a, and the corresponding concentrations of SRB are shown in Figure 5b. The time scales in parts a and b of Figure 5 are extended to 240 days to better illustrate the trends. As shown in Figure 5a, the percentage of initial cellulose remaining at 124 days

FIGURE 2. Comparison of experimental and simulated concentrations based on Contois decomposition kinetics for batch test 1: (a) ferrous iron and (b) hydrogen sulfide concentrations vs time (k_c = decomposition rate coefficient; K_c = half-saturation coefficient; $[X_d]/[CE]$ = initial concentration ratio of decomposer bacteria to polysaccharide).

(i.e., SO_4^{2-} depletion) ranges from 40 to 60%, depending on the value for $[X_d]/[CE]$. The simulations shown in Figure 5b illustrate the succession of different phases in the dynamics of the SRB population, which is expected based on bacterial growth on limiting substrates (25). The early lag-growth stage agrees with the initial lag in the growth of cellulose decomposers and low initial rates of cellulose decomposition and sulfate reduction. The brief stationary phase in SRB dynamics corresponds to equilibrium between Monod growth based on SO_4^{2-} and lactate ($C_3H_5O_3^-$) and first-order decay. As SO_4^{2-} approaches depletion near 124 days, the rate of growth decreases until a point when the population undergoes purely exponential decay. The stationary phase would be expected to be longer in scenarios with replenishment of SO_4^{2-}, such as general field applications of SR systems for AMD remediation or replenished flow-through experiments. In those cases, the decay phase probably would be more gradual and caused by increasing $C_3H_5O_3^-$ scarcity in the system rather than SO_4^{2-} depletion.

Batch Test 2. The simulated results of batch test 2 (batch mixture 3 in ref 9) containing decomposable, composted leaf mulch at an estimated initial concentration of 22.3 g/L are compared to the experimental results as shown in Figures 6−8. Simulated concentrations for SO_4^{2-} and Fe^{2+} vs batch reaction time are obtained considering the Contois model for the decomposition of polysaccharides, Monod kinetics for lactate-based sulfate reduction, and instantaneous pre-
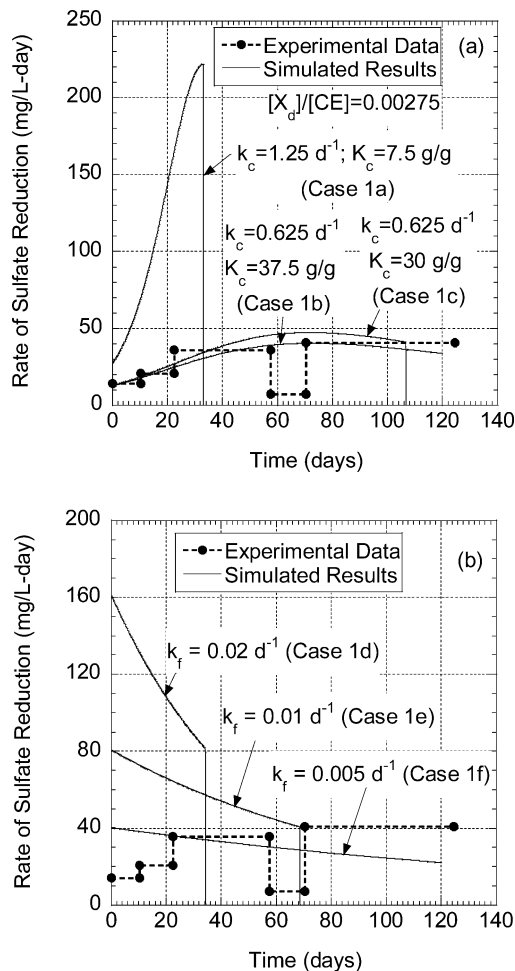
FIGURE 3. Comparison of experimental and simulated rates of sulfate reduction versus time for batch test 1: (a) Contois decomposition kinetics and (b) first-order decomposition kinetics (k_c = decomposition rate coefficient; K_c = half-saturation coefficient; $[X_d]/[CE]$ = initial concentration ratio of decomposer bacteria to polysaccharide; k_f = first-order decomposition rate coefficient).
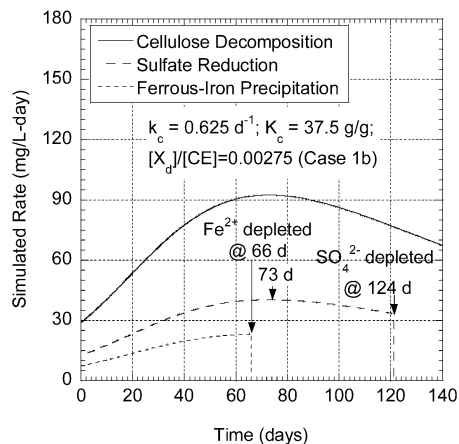

FIGURE 4. Simulated results for batch test 1, rates of cellulose decomposition, sulfate reduction, and ferrous iron precipitation vs time (k_c = decomposition rate coefficient; K_c = half-saturation coefficient; $[X_d]/[CE]$ = initial concentration ratio of decomposer bacteria to polysaccharide).

cipitation of FeS. Results for H_2S are not given in ref 9 for this batch test.

Sulfate and Ferrous Iron. Simulated SO_4^{2-} and Fe^{2+} concentrations based on Contois kinetics for a range of values
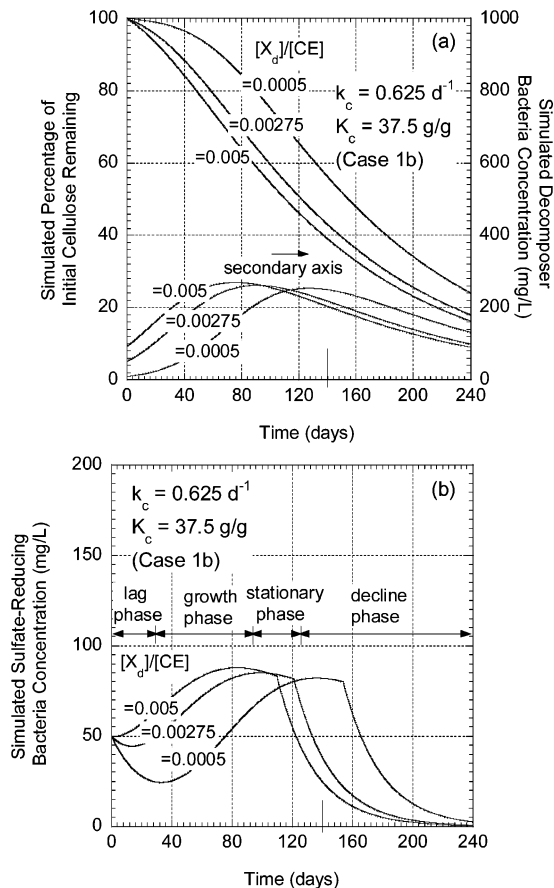
FIGURE 5. Simulated results for batch test 1: (a) percentage of initial cellulose and decomposer bacteria concentrations and (b) concentrations of SRB (k_c = decomposition rate coefficient; K_c = half-saturation coefficient; $[X_d]/[CE]$ = initial concentration ratio of decomposer bacteria to polysaccharide).

for $[X_d]/[CE]$ are compared to experimental results in Figure 6. The best comparisons for the SO_4^{2-} concentrations are obtained with $[X_d]/[CE]$ = 0.01 (case 2a) or with $[X_d]/[CE]$ = 0.005 (case 2b). However, with respect to the approximation of Fe^{2+}, instantaneous precipitation with the same $[X_d]/[CE]$ ratios used for SO_4^{2-} results in simulated Fe^{2+} concentrations that decline faster than occur for the experimental data. Therefore, FeS precipitation appears to follow slower kinetics than instantaneous precipitation. In this case, kinetically controlled precipitation of FeS, rather than instantaneous precipitation, may be more appropriate to approximate the observed Fe^{2+} data. For this reason, kinetically controlled precipitation of iron sulfide will be used subsequently to model the data from batch tests 3 and 4. The results also suggest that the consideration of any additional sink for Fe^{2+}, such as siderite ($FeCO_3$) precipitation, would cause the simulated behavior of Fe^{2+} to deviate even more from the experimental data.

On the basis of the decomposition parameter values for the leaf mulch of batch test 2, the leaf mulch is more degradable than the cellulose in batch test 1. This consideration is in agreement with the earlier depletion of SO_4^{2-} in batch test 2 (i.e., at 65 days, as opposed to 124 days in batch test 1) and can be explained by the difference in the nitrogen content of the two materials. The leaf mulch is reported to have a carbon-to-nitrogen ratio of 21 (9), which is within the range of values associated with more easily degradable materials (27). The cellulose in batch test 1 is
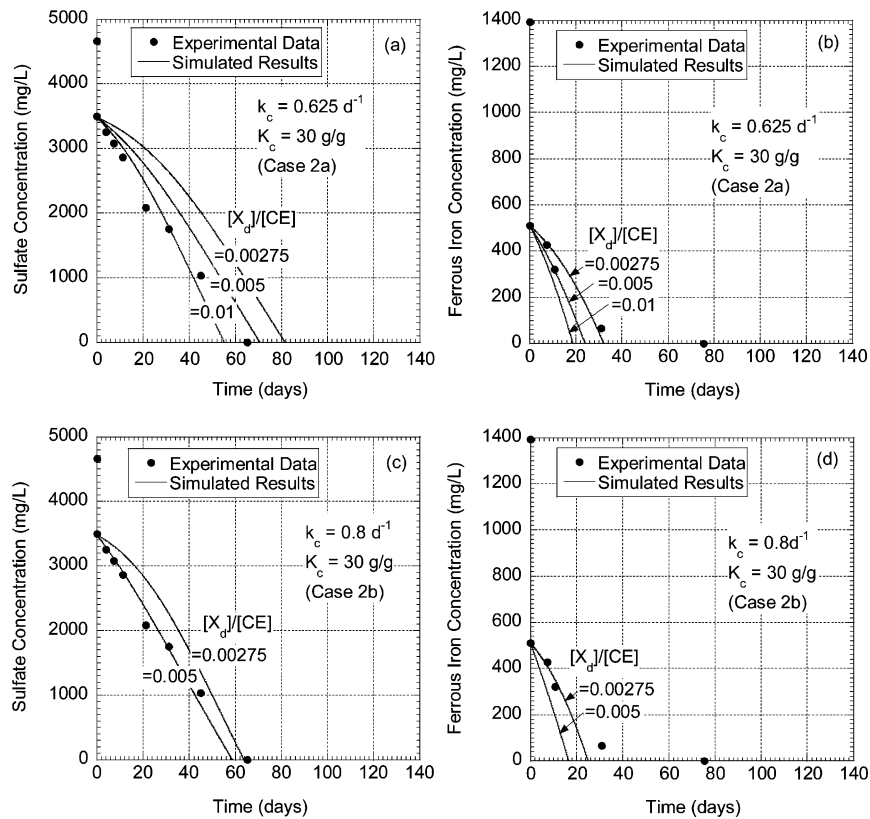
FIGURE 6. Comparison of experimental and simulated sulfate and ferrous iron concentrations for batch test 2 based on different Contois decomposition kinetics (k_c = decomposition rate coefficient; K_c = half-saturation coefficient; $[X_d]/[CE]$ = initial concentration ratio of decomposer bacteria to polysaccharide).
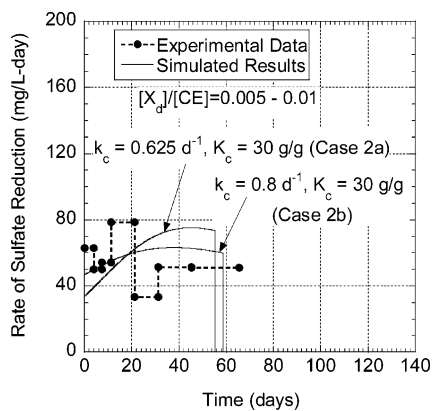

FIGURE 7. Comparison of simulated and experimental rates of sulfate reduction for batch test 2, with different Contois decomposition kinetics (k_c = decomposition rate coefficient; K_c = half-saturation coefficient; $[X_d]/[CE]$ = initial concentration ratio of decomposer bacteria to polysaccharide).

reported to lack in nitrogen (*9*), a condition that makes decomposer colonization and activity more difficult.

Rates of Sulfate Reduction. Simulated rates of sulfate reduction with time are compared in Figure 7 to values calculated from the $SO_4{}^{2-}$ data given in ref *9* considering Contois decomposition kinetics (cases 2a and 2b). In this case, the maximum rate of sulfate reduction occurs several days after the beginning of the experiment, which compares reasonably well with the experimental data. In contrast, the use of first-order decomposition kinetics would result in the maximum rate of sulfate reduction occurring at time zero, as previously shown and discussed for batch test 1.

Polysaccharide, Decomposer Bacteria, and SRB. On the basis of the parameter values for Contois decomposition kinetics (cases 2a and 2b, Table 3), the simulated percentages of the initial decomposable polysaccharide remaining and concentrations of decomposer bacteria as well as the simulated concentrations of SRB are shown in Figure 8, with time scales extended to 240 days to better illustrate the trends. The percentage of initial polysaccharide remaining at 65 days (i.e., $SO_4{}^{2-}$ depletion) ranges from 55 to 75% (case 2a), and 50−60% (case 2b), depending on the value for $[X_d]/[CE]$. The SRB concentrations in this experiment are higher than those in batch test 1, which is in agreement with faster leaf mulch degradation kinetics, but earlier depletion of $SO_4{}^{2-}$ (i.e., at 65 days instead of 124 days) causes the SRB stationary phase to be negligible, i.e., the population enters an exponential decay due to $SO_4{}^{2-}$ depletion before the time that would be required for the stationary phase to be achieved.

Batch Test 3. The simulated results of batch test 3 (batch mixture 6 in ref *9*) containing decomposable, composted leaf mulch and maple sawdust at estimated initial concentrations of 13.3 and 8.9 g/L, respectively, are compared to the experimental results in Figures 9 and 10. Simulated concentrations for $SO_4{}^{2-}$ and Fe^{2+} vs batch reaction time are obtained considering a Contois kinetic model for the decomposition of polysaccharides, Monod kinetics for lactate-based sulfate reduction, and both instantaneous and kinetically controlled precipitation of FeS. Two decomposer populations are assumed, each population directly associated with a decomposing material, and the amounts of lactate produced in solution over time include contributions from the two decompositions. The concentrations of H_2S, polysaccharides, and bacterial populations are not shown because simulated results are similar to those shown for batch tests 1 and 2.
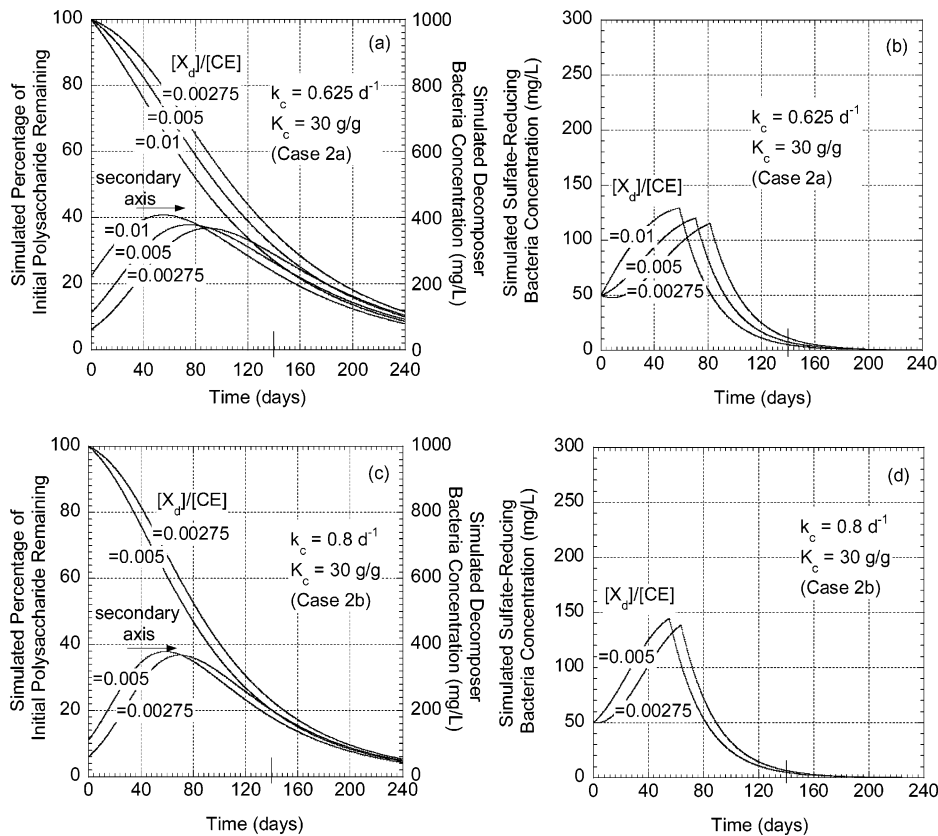
FIGURE 8. Simulated percentages of initial polysaccharide, decomposer, and SRB concentrations for batch test 2 based on different Contois decomposition kinetics (k_c = decomposition rate coefficient; K_c = half-saturation coefficient; $[X_d]/[CE]$ = initial concentration ratio of decomposer bacteria to polysaccharide).
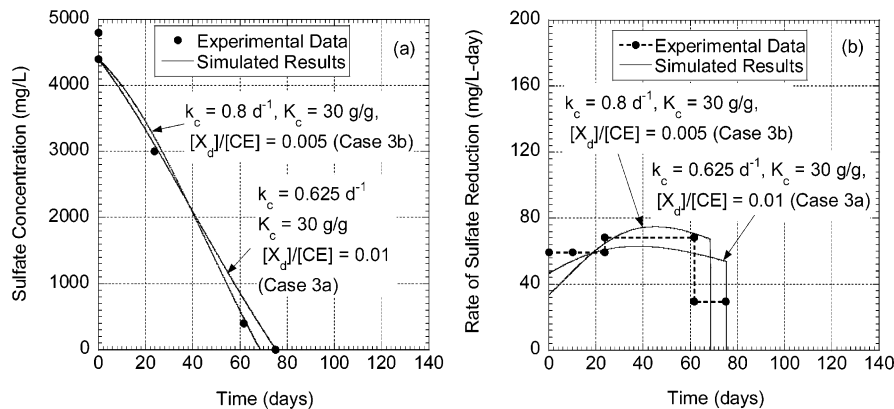

FIGURE 9. Comparison of experimental data and simulated results for batch test 3 based on different Contois decomposition kinetics (k_c = decomposition rate coefficient; K_c = half-saturation coefficient; $[X_d]/[CE]$ = initial concentration ratio of decomposer bacteria to polysaccharide).

Sulfate and Rates of Sulfate Reduction. Simulated SO_4^{2-} concentrations and rates of sulfate reduction are compared to experimental results in Figure 9. Leaf mulch decomposition kinetics is assumed to be equal to that in batch test 2, and the parameter values for sawdust decomposition are adjusted. As shown in Figure 9, the simulated SO_4^{2-} concentrations and rates of sulfate reduction with time compare well with the experimental data, i.e., when sawdust decomposition is assumed equal to that of leaf mulch (see Table 3). Although wood usually is expected to be more recalcitrant than leaf detritus, the sawdust is characterized by fine gradation and high specific surface area, factors that enhance degradability (46), and may assist in the decomposition of the sawdust.

Ferrous Iron and Rates of Precipitation. Simulated Fe^{2+} concentrations and rates of Fe^{2+} precipitation with time are compared to experimental results in Figure 10 based on both instantaneous precipitation of FeS and kinetically controlled precipitation with rate constants, k, of 0.1 and 0.0005 d^{-1}. As shown in Figure 10, both instantaneous precipitation of FeS and kinetically controlled precipitation with $k = 0.1$ d^{-1} are equivalent in terms of Fe^{2+} concentrations and rates of Fe^{2+} precipitation, indicating that the rate constant of 0.1 d^{-1} is essentially equivalent to instantaneous precipitation in this system. However, the best approximation of Fe^{2+} concentrations and rates of Fe^{2+} precipitation is obtained when the precipitation of FeS is more kinetically limited with $k = 0.0005$ d^{-1}. This kinetic limitation to FeS precipitation also was previously observed for the comparisons based on batch test 2.
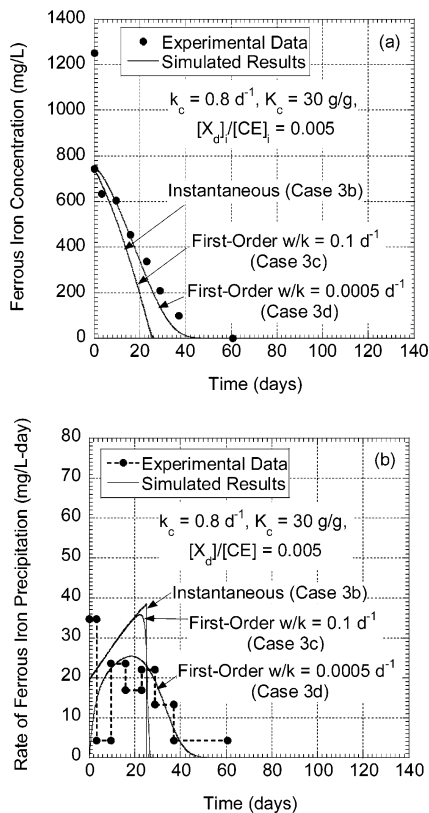
FIGURE 10. Comparison of experimental data and simulated results for batch test 3 based on different Contois decomposition kinetics and assuming instantaneous or first-order precipitation (k_c = decomposition rate coefficient; K_c = half-saturation coefficient; $[X_d]/[CE]$ = initial concentration ratio of decomposer bacteria to polysaccharide; k = first-order precipitation rate coefficient).

As shown in Figure 10, the initial rate of Fe^{2+} precipitation with $k = 0.1$ d^{-1} is significantly higher than that associated with $k = 0.0005$ d^{-1} (i.e., 20 mg/L·day vs 1 mg/L·day), but the maximum rate of Fe^{2+} precipitation with $k = 0.1$ d^{-1} is only ~30% higher than the maximum rate associated with $k = 0.0005$ d^{-1} (i.e., 36 mg/L·day vs 25 mg/L·day). The results show that the rates of Fe^{2+} precipitation with time are not directly proportional to the precipitation rate constant. The lack in proportionality is caused by the differences in H_2S concentrations in solution. For example, H_2S concentrations at 7 days are in the order of 40 mg/L for the case with $k = 0.0005$ d^{-1} but only 0.3 mg/L for the case with $k = 0.1$ d^{-1}. Higher levels of H_2S in solution increase the rate of Fe^{2+} precipitation and, therefore, cause the rates of Fe^{2+} precipitation to increase for the case with $k = 0.0005$ d^{-1}.

Batch Test 4. The simulated results of batch test 4 (batch mixture 7 in ref 9) containing decomposable leaf mulch, sawdust, wood chips, and sewage sludge at estimated initial concentrations of 19.1, 3.2, 4.8, and 1.1 g/L, respectively, are compared to the experimental results as shown in Figure 11. Simulated concentrations for SO_4^{2-} vs batch reaction time are obtained considering a Contois kinetic model for the decomposition of polysaccharides and Monod kinetics for lactate-based sulfate reduction. In this test, experimental Fe^{2+} results are neglected due to the decline of more than 90% of the initial concentration of Fe^{2+} occurring at time zero, which is assumed not to be related to the biochemistry of SR systems based on decomposable solid materials. The concentrations of H_2S, polysaccharides, and bacterial populations are not shown because simulated results are similar to those shown for batch tests 1 and 2. Leaf mulch and sawdust are grouped as a single decomposable material, and therefore, three different decomposable materials are considered (i.e., leaf mulch/sawdust, wood chips, and sewage sludge). Accordingly, three populations of decomposer bacteria are assumed, each population associated to one of the substrates (see Supporting Information).

Sulfate and Rates of Sulfate Reduction. Both simulated SO_4^{2-} concentrations and rates of sulfate reduction are compared to experimental results in parts a and b of Figure 11, where the experimental sulfate reduction rates were calculated from the SO_4^{2-} data given in ref 9, for the range of parameter values shown. Leaf mulch and sawdust decomposition kinetics were assumed to be the same as for batch tests 2 and 3, and the parameter values for wood chips were adjusted. As shown in Figure 11a, the simulated SO_4^{2-} concentrations with time compare well with the experimental data for both cases shown (cases 4a and 4b).

The results for cases 4c and 4d shown in Figure 11b were obtained by isolating the contribution of the sewage sludge to the rate of sulfate reduction. Accordingly, the rates of sulfate reduction associated with cases 4b, 4c, and 4d are compared in Figure 11b. Case 4b provides a good approximation to the experimental rates of sulfate reduction, whereas cases 4c (including all organic substrates except for sewage sludge) and 4d (only including sewage sludge) provide poorer approximations. A comparison of the simulated rates obtained in cases 4b, 4c, and 4d illustrates the role of the easily degradable material in boosting the initial rates of sulfate reduction. However, the results for case 4d indicate that sulfate reduction based on sewage sludge alone would decline quickly (i.e., the rate declines by more than 2 mg/L·day every day after 5 days) and, therefore, the SR system requires materials that degrade more slowly in order to sustain sulfate reduction.
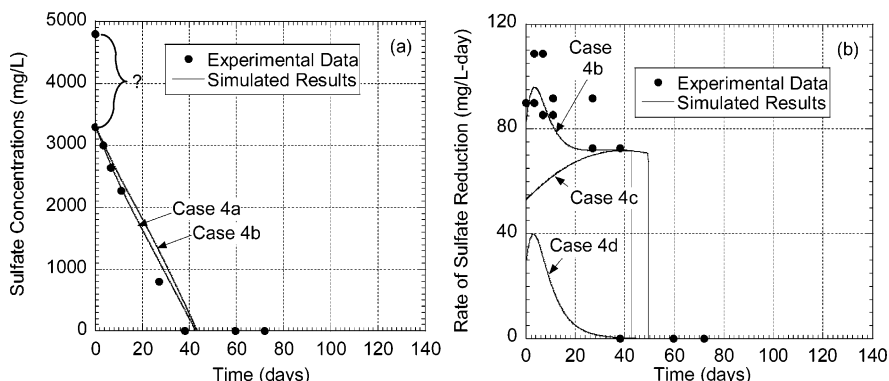

FIGURE 11. Comparison of experimental and simulated sulfate concentrations and rates of sulfate reduction for batch test 4 (refer to Table 3 for parameter values for cases 4a–4d).

Supporting Information Available

Information regarding the conceptual basis for the model, model equations, mathematical solution, mass balance, and local truncation errors for the modeling simulations. This material is available free of charge via the Internet at http:// pubs.acs.org.

Literature Cited

(1) Tuttle, J. H.; Dugan, P. R.; Randles, C. I. Microbial sulfate reduction and its potential utility as an acid mine water pollution abatement procedure. *Appl. Microbiol.* **1969**, *17* (2), 297−302.

(2) Wakao, N.; Takahashi, T.; Sakurai, Y.; and Shiota, H. A treatment of acid mine water using sulfate-reducing bacteria. *J. Ferment. Technol.* **1979**, *57* (5), 445−452.

(3) Dvorak, D. H.; Hedin, R. S.; Edenborn, H. M., McIntire, P. E. Treatment of metal-contaminated water using bacterial sulfate reduction: results from pilot-scale reactors. *Biotechnol. Bioeng.* **1992**, *40* (5), 609−616.

(4) Hammack, R. W.; Edenborn, H. M. Treatment of water from an open pit copper mine using biogenic sulfide and limestone: a feasibility study. *Appl. Microbiol. Biotechnol.* **1992**, *37* (5), 674−678.

(5) Bechard, G.; Yamazaki, H.; Gould, W. D.; Bedard, P. Use of cellulosic substrates for the microbial treatment of acid mine drainage. *J. Environ. Qual.* **1994**, *23* (1), 111−116.

(6) Christensen, B.; Laake, M.; Lien, T. Treatment of acid mine water by sulfate-reducing bacteria; results from a bench scale experiment. *Water Research* **1996**, *30* (7), 1617−1624.

(7) Prasad, D.; Wai, M.; Berube, P.; Henry, J. G. Evaluating substrates in the biological treatment of acid mine drainage. *Environ. Technol.* **1999**, *20* (5), 449−458.

(8) Chang, I. S.; Shin, P. K.; Kim, B. H. Biological treatment of acid mine drainage under sulphate-reducing conditions with solid waste materials as substrates. *Water Res.* **2000**, *34* (4), 1269−1277.

(9) Waybrant, K. R.; Blowes, D. W.; Ptacek, C. J. Selection of reactive mixtures for use in permeable reactive walls for treatment of mine drainage. *Environ. Sci. Technol.* **1998**, *32* (13), 1972−1979.

(10) Waybrant, K. R.; Ptacek, C. J.; Blowes, D. W. Treatment of mine drainage using permeable reactive barriers: column experiments. *Environ. Sci. Technol.* **2002**, *36* (6), 1349−1356.

(11) Cocos, I. A.; Zagury, G. J.; Clement, B.; Samson, R. Multiple factor design for reactive mixture selection for use in reactive walls in mine drainage treatment. *Water Res.* **2002**, *36* (1), 167−177.

(12) Hulshof, A. H.; Blowes, D. W.; Ptacek, C. J.; Gould, W. D. Microbial and nutrient investigations into the use of in situ layers for treatment of tailings effluent. *Environ. Sci. Technol.* **2003**, *37* (21), 5027−5033.

(13) Frommichen, R.; Kellner, S.; Friese, K. Sediment conditioning with organic and/or inorganic carbon sources as a first step in alkalinity generation of acid mine pit lake water (pH 2−3). *Environ. Sci. Technol.* **2003**, *37* (7), 1414−1421.

(14) Hammack, R. W.; Edenborn, H. M.; Dvorak, D. H. Treatment of water from an open pit copper mine using biogenic sulfide and limestone: a feasibility study. *Water Resour.* **1994**, *28* (11), 2321−2329.

(15) Benner, S. G.; Blowes, D. W.; Gould, W. D.; Herbert, R. B.; Ptacek, C. J. Geochemistry of a permeable reactive barrier for metals and acid mine drainage. *Environ. Sci. Technol.* **1999**, *33* (16), 2793−2799.

(16) Benner, S. G.; Gould, W. D.; Blowes, D. W. Microbial populations associated with the generations and treatment of acid mine drainage. *Chem. Geol.* **2000**, *169* (3−4), 435−448.

(17) Blowes, D. W.; Ptacek, C. J.; Benner, S. G.; McRae, C. W. T.; Bennett, T. A.; Puls, R. W. Treatment of inorganic contaminants using permeable reactive barriers. *J. Contam. Hydrol.* **2000**, *45* (1−2), 123−137.

(18) Steed, V.; Suidan, M.; Gupta, M.; Miyahara, T.; Acheson, C.; Sayles, G. Development of a sulfate-reducing biological process to remove heavy metals from acid mine drainage. *Water Environ. Res.* **2000**, *72* (5), 530−535.

(19) Ludwig, R. D.; McGregor, R. G.; Blowes, D. W.; Benner, S. G.; Mountjoy, K. A permeable reactive barrier for treatment of heavy metals. *Ground Water* **2002**, *40* (1), 59−66.

(20) Boudreau, B. P.; Westrich, J. T. The dependence of bacterial sulfate reduction on sulfate concentration in marine environments. *Geochim. Cosmochim. Acta* **1984**, *48* (12), 2503−2516.

(21) Westrich, J. T.; Berner, R. A. The role of sedimentary organic matter in bacterial sulfate reduction: the G model tested. *J. Limnol. Oceanogr.* **1984**, *29* (2), 236−249.

(22) Drury, J. W. Modeling of sulfate reduction in anaerobic solid substrate bioreactors for mine drainage treatment. *Mine Water Environ.* **2000**, *19* (1), 18−28.

(23) Janssen, B. H. A simple method for calculating decomposition and accumulation of young soil organic matter. *Plant Soil* **1984**, *76* (1−3), 297−304.

(24) Middelburg, J. J. A simple rate model for organic matter decomposition in marine sediments. *Geochim. Cosmochim. Acta* **1989**, *53* (7), 1577−1581.

(25) Monod, J. The growth of bacterial cultures. *Annu. Rev. Microbiol.* **1949**, *3*, 371−394.

(26) Gujer, W.; Zehnder, A. J. Conversion processes in anaerobic digestion. *Water Sci. Technol.* **1983**, *15* (8−9), 127−167.

(27) Chynoweth, D. P.; Pullammanappallil, P. Anaerobic digestion of municipal solid waste. In *Microbiology of Solid Waste*; Palmasano, A., Barlaz, M. A., Eds.; CRC Press: Boca Raton, FL, 1996; pp 77−113.

(28) Mayer, K. U.; Frind, E. O.; Blowes, D. W. Multicomponent reactive transport modeling in variably saturated porous media using a generalized formulation for kinetically controlled reactions. *Water Resour. Res.* **2002**, *38* (9), 13−1 to 13-21.

(29) Prommer, H.; Barry, D. A.; Chiang, W. H.; Zheng, C. PHT3D-A MODFLOW-MT3DMS-based reactive multicomponent transport model. In *MODFLOW 2001 and Other Modeling Odysseys*; Seo, H., Poeter, E., Zheng, C., Eds.; International Groundwater Modeling Center, Colorado School of Mines: Golden, CO, 2001; pp 477−483.

(30) Harbaugh, A. W.; Banta, E. R.; Hill, M. C.; McDonald, M. G. *MODFLOW-2000, the U. S. Geological Survey Modular Groundwater Model - User Guide to Modularization Concepts and the Groundwater Flow Process*; USGS Open-File Report 00-92, 2000.

(31) Zheng, C.; Wang, P. P. *MT3DMS: A Modular Three-Dimensional Multispecies Model for Simulation of Advection, Dispersion, and Chemical Reactions of Contaminants in Groundwater Systems; Documentation and User's Guide*; U.S. Army Corps of Engineers, Contract Report SERDP-99-1, 1999.

(32) Parkhurst, D. L.; Appelo, C. A. *User's Guide to PHREEQC − A Computer Program for Speciation, Batch Reaction, One-Dimensional Transport, and Inverse Geochemical Calculations*; Technical Report 4227, U.S. Geological Survey, 1999.

(33) Benner, S. G.; Blowes, D. W.; Ptacek, C. J.; Mayer, K. U. Rates of sulfate reduction and metal sulfide precipitation in a permeable reactive barrier. *Appl. Geochem.* **2002**, *17* (1), 301−320.

(34) Amos, R. T.; Mayer, K. U.; Blowes, D. W.; Ptacek, C. J. Reactive transport modeling of column experiments for remediation of acid mine drainage. *Environ. Sci. Technol.* **2004**, *38* (11), 3131−3138.

(35) Sposito, G. *The Chemistry of Soils*; Oxford University Press: Oxford, UK, 1989.

(36) Widdel, F. Microbiology and ecology of sulfate reducing bacteria. In *Biology of Anaerobic Microorganisms*; Zehnder, A. J. B., Ed.; Wiley-Interscience: New York, 1988; Chapter 10, pp 469−585.

(37) Postgate, J. R. *The Sulphate-Reducing Bacteria*, 2nd ed.; Cambridge University Press: Cambridge, UK, 1984.

(38) Fenchel, T.; Harrison, P. The significance of bacterial grazing and mineral cycling for the decomposition of particulate detritus. In *The Role of Terrestrial and Aquatic Organisms in Decomposition Processes*; Anderson, J. M. A., Macfadyen, Eds.; Blackwell Scientific Publications: Oxford, UK, 1976; pp 285−299.

(39) Henriksen, T. M.; Breland, T. A. Carbon mineralization, fungal and bacterial growth, and enzyme activities as affected by contact between crop residues and soil. *Biol. Fertilization Soils* **2002**, *35* (1), 41−48.

(40) Vavilin, V. A.; Rytov, S. V.; Lokshina, L. A description of hydrolysis kinetics in anaerobic degradation of particulate organic matter. *Bioresour. Technol.* **1996**, *56* (1), 229−237.

(41) Okabe, S.; Characklis, W. G. Effects of temperature and phosphorous concentration on microbial sulfate reduction by *Desulfovibrio desulfuricans*. *Biotechnol. Bioeng.* **1992**, *39* (10), 1031−1042.

(42) Okabe, S.; Nielsen, P. H.; Characklis, W. G. Factors affecting microbial sulfate reduction by *Desulfovibrio desulfuricans* in

continuous culture: limiting nutrients and sulfide concentration. *Biotechnol. Bioeng.* **1992**, *40* (6), 725−734.

(43) Konishi, Y.; Yoshida, N.; Asai, S. Desorption of hydrogen sulfide during batch growth of the sulfate-reducing bacterium *Desulfovibrio desulfuricans. Biotechnol. Prog.* **1996**, *12* (3), 322−330.

(44) Middleton, A. C.; Lawrence, A. W. Kinetics of microbial sulfate reduction. *J. Water Pollut. Control Fed.* **1977**, *49* (7), 1659−1670.

(45) Rittman, B. E.; McCarty, P. L. *Environmental Biotechnology: Principles and Applications*; McGraw-Hill: New York, 2001.

(46) Humphrey, A. E. The hydrolysis of cellulosic materials to useful products. In *Hydrolysis of Cellulose: Mechanisms of Enzymatic and Acid Catalysis*, Advances in Chemistry Series, No. 181, American Chemical Society: Washington D. C., 1979; Chapter 2, pp 25−53.